RESEARCH ON MEASUREMENT METHOD FOR THE CORE FLOW DISTRIBUTION EXPERIMENT IN MOLTEN SALT REACTORS BASED ON CONDUCTIVITY FLUID TRACKING TECHNOLOGY

Maoying Xu[1,2], Jian Tian[1,2], Yu shuang Chen[1,2], Chong Zhou[1,2], Yang Zou[1,2]*

[1] *Shanghai Institute of Applied Physics, Chinese Academy of Sciences, Shanghai, 201800, China*
[2] *University of Chinese Academy of Sciences, No.19A Yuquan Road, Shijingshan District, Beijing, China*
* *tianjian@sinap.ac.cn*

Keywords: MOLTEN SALT REACTOR, FLOW DISTRIBUTION EXPERIMENTS, FLOW MEASUREMENT METHOD, CONDUCTIVITY LIQUID TRACKING

Abstract

Measurement of flow distribution in core is an important engineering validation experiment during the design process of a new-type nuclear reactor. To accurately measure the flow rate in each channel of the molten salt reactor core model, a novel measurement method of flow based on conductivity liquid tracking is proposed in this study. The measurement method is executed by injecting conductivity liquid into the channel with flowing pure water and tracking the fluid cluster of conductivity liquid, then the flow rate of the electrolyte cluster in the channel can be obtained through monitoring the conductivity variation as the electrolyte cluster passes the detector built-in the flow passage. After the calibration of the flow rate from tracking electrolyte cluster with intrinsic relationship previously verified, the flow rate of bulk fluid in the channel can be obtained. Computational fluid dynamics (CFD) simulations confirmed that the results obtained from the current measurement method align well with the normative flow rates, with a maximum deviation of 1.26%, which provides the feasibility for the calibration of the measurement method. Extensive promotion of the current method to all kinds of channels enables the measurement of flow distribution of the molten salt reactor core. The ongoing development and research of the method can provide effective tools for future flow distribution experiments of molten salt reactor core.

1. Introduction

With the development of the global economy, the gap between human energy demand and supply continues to widen. And with the growing environmental awareness, cleaner and more efficient energy sources are increasingly becoming the preferred option for both industrial production and daily life. Nuclear energy, as a pivotal element in the emerging energy landscape, is playing an increasingly important role. Among them, the molten salt reactor (MSR), one of the fourth-generation reactors, plays a more significant role due to its use of thorium fuel, which is abundant in China. Moreover, the molten salt both serves as coolant and fuel, which achieving higher temperatures and lower pressures compared to pressurized water reactors, thereby offering enhanced economic and safety benefits. Consequently, MSR is recognized as one of the key directions for the future development of nuclear energy in China[1, 2].

The thermal-hydraulic design of the reactor core is a critical component in reactor research, as it is crucial for the safe and effective transfer of heat within the reactor core. Verifying the validity of the reactor core's thermal-hydraulic design is an essential task to ensure the reactor's safe operation. Due to the complexity of the channel structures and flow boundaries within the reactor, the flow distribution data cannot be obtained through analytical methods. Despite numerical calculations can obtain the flow distribution through directly modelling, deviations may still exist between the analysis results and actual situation due to simplification and inaccuracy of analysis model. At present, verification experiments are still an indispensable means for assessing the reactor's hydraulic design. Performing model experiments and obtaining the flow distribution of all channels within the reactor core will serve as a reliable basis for validating the hydraulic structural design of the reactor prototype and provide crucial parameter inputs for the thermal-hydraulic analysis of the reactor core.

MSRs adopt a completely new design concept, making the thermal-hydraulic of the reactor become one of the important research contents. Therefore, the core flow distribution experiment appears to be particularly crucial for the research of MSR. Historically, core flow distribution experiments typically employed scaled models of the reactor to investigate the hydraulic characteristics of the reactor prototype[3, 4]. For instance, a 1:6 scaled model hydraulic simulation test was conducted for the CAP1400 reactor [5, 6], a 1:3 scaled model integral hydraulic simulation test was conducted in the design of China National Nuclear Corporation's modular advanced small pressurized water reactor “Linglong-1” (ACP100) [7], a 1:5 scaled model overall hydraulic simulation test was carried out in the advanced megawatt-class pressurized water reactor ACPR1000 design developed by the Guangdong Nuclear Power Group (GNPG)[8], a 1:1 model integral hydraulic simulation test was conducted in China Advanced Research

Reactor (CARR) Designs[9] and a 1:5 scaled model integral hydraulic simulation test was conducted for the APR1400 reactor design in South Korea[10, 11]. These flow distribution tests typically employed a reactor model with a single type of circular flow channel to modeling the assembly, where the attribute of fungible channels are suitable for the use of traditional methods for the flow measurement. For example, the core inlet flow distribution experiment for the Qinshan Phase II 600 MW reactor used a custom internal magnetic turbine flow meter for measuring flow[12-14]. Similarly, the core inlet flow distribution test for the CAP1400 reactor used conventional flow meters to measure the flow rate of core component[15]. In sodium-cooled reactor research, flow rates have also been indirectly obtained by measuring pressure drops[16].Unlike the reactors discussed earlier, the flow paths of reactor core are more complex and diverse in MSR core. In addition to traditional circular channels, stadium-shaped and annular channels are also included. These unique flow channels currently lack conventional, effective flow measurement methods. Furthermore, when the MSR core flow distribution experiment is carried out, the confined space between channels limits the application of traditional flow measurement methods which often require large components or modifications to the channels.

In this study, a specialized flow measurement method is introduced to overcome the flow measurement challenges of MSR core models. Multiple advantages such as simple components, small size, applicability to various channel shapes, and minimal impact on the flow field within the channels, are offered to satisfy the strict requirements of flow distribution measurements of MSR core hydraulic experiment. This paper is structured as follows: Firstly, theoretical principles of the method were discussed. Secondly, the feasibility was assessed through gradual advancement including experiments examining, data processing，as well as CFD simulation verification. Finally, based on the analysis results, potential optimization directions for the method were proposed.

2. Method of measurement

Deionized water is typically employed as the bulk fluid in the current flow measurement. Under steady-state flow conditions, a quantified amount of electrolyte solution is introduced into the deionized water. By tracking the transport of the electrolyte solution within the flow channels, the flow velocity of the electrolyte solution can be determined. Based on the calibrated correlation between the velocity of electrolyte solution and the bulk flow of fixed channel, the average velocity of the channel flow can be determined, from which the volumetric and mass flow rate within the channel can be calculated.

The schematic of the conductivity liquid tracking method is shown in Figure 1. Two detectors with a certain distance are built in the channel to be measured. Initially, deionized water is flowing in the channel, then electrolyte solution is injected and follow the mainstream flow through the channel. By measuring the flow time of the labelled fluid cluster to pass between two detectors and performing subsequent calculations, the flow velocity of the labelled fluid cluster can be determined. The velocity of the electrolyte cluster can be represented as：

$$v_e = \frac{L}{\Delta t} \tag{1}$$

Here， L represents the distance of two detectors, Δt represents the time difference of labelled fluid cluster flowing pass the two detector.

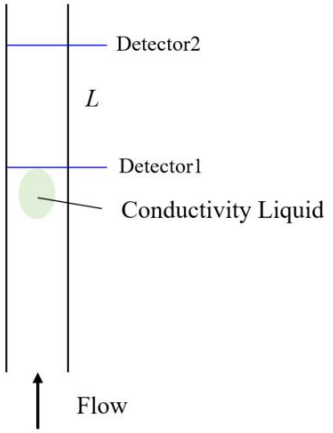

Fig. 1 Measurement Schematic DiagramAs the labelled fluid cluster migrates in conjunction with the bulk flow, the velocity of the labelled fluid cluster can serve as an indicator of the bulk flow velocity. A characteristic relationship exists between the velocity of the labelled fluid cluster and the average velocity of the bulk flow within the channel:

$$v = f(v_e) \tag{2}$$

Given that the injected electrolyte has a small mass and relatively low concentration, and the density ρ of bulk fluid can be assumed constant. Therefore, the mass flow rate in the channel can be calculated using the following equation:

$$q_m = \rho \times A \times f(v_e) \tag{3}$$

In the equation, q_m represents the average mass flow rate of the channel, ρ is the fluid density, is the cross-sectional area of the channel.

The tracking of the electrolyte fluid within the channel is mainly accomplished by measuring the electrical conductivity of the fluid. As a labelled fluid cluster passes through a measurement point defined by a linear probe, an appreciable electrical conduction response can be given rise. Owing to the differences in electrical conductivity at spatial variations within the cluster, a conductivity signal over time is generated at the measurement point when the cluster passes through a detector, typically exhibiting a rise from baseline to a peak and then returning to baseline. By data processing of the overall conductivity signals recorded at two separate measurement points, the time interval, Δt as shown in formula (1), of labelled fluid cluster passing though the detector can be recorded.

Before application of current method to actual measurements, some in-depth studies of key issues needs to be conducted. Firstly, the availability of tracking electrolyte solution with conductivity measurement of fluid need and the need to be confirmed. Secondly, the analytical methods to extract the time interval from two separate conductivity signals needs to be further optimized. Additionally, detailed assessments of factors which may affect the measurement results are required.

Furthermore, it is necessary to verify the relationship between the flow velocity of the labelled clusters and the velocity of bulk fluid. After all the above studies are done, potential optimizations of current method should be proposed.

3. Analysis of Measurement

3.1 Relationship between conductivity and the concentration of the conductive solution

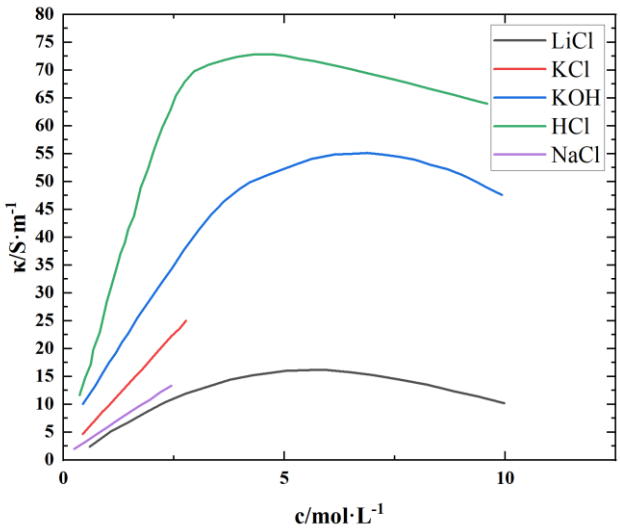

Fig. 2. Graphs of Conductivity as a Function of Concentration for Various Electrolyte Solutions

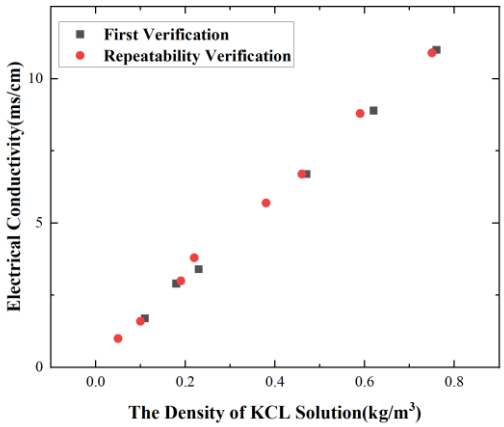

Fig. 3 The Variation of Conductivity with Concentration for KCl Solution from Experiment

The relationship between the conductivity of an electrolyte solution and its concentration typically exhibits a curve with a peak value. At low concentrations, the increase in ion quantity is the dominant factor, resulting in a rise in conductivity. Therefore, to maintain a one-to-one correspondence between conductivity and concentration, the method requires using a low-concentration electrolyte solution as the conductivity tracking. As illustrated in the figure 2 [17, 18], the conductivity of KCl solution exhibits a strong linear correlation with concentration in the low-concentration range. Furthermore, KCl is safe, no strong corrosive, and widely used as a standard chemical reagent for calibrating electrical conductivity, making it an ideal choice for use as the electrolyte. Previous literature has reported experimental investigations on the relationship between the conductivity and concentration of KCl solutions [19]. Measurements are conducted to confirm in this study as shown in figure 3, results were consistent with the trend shown in figure 2 and exhibit a linear trend. Hence, the labelled fluid cluster can be effectively tracked using conductivity measurements.

3.2 Data processing to extract the flow time of conductive solution

Direct application of this measurement method yields curves such as those presented in Figure 4. The blue curve depicts the conductivity signal, denoted as x(t), measured on the x radial line at Point 1. The red curve represents the conductivity signal, denoted as y(t), measured on the x radial line at Point 4. Due to the tendency of the electrolyte to diffuse radially outward from the center within a cluster, the mass fraction of the electrolyte at the head and tail of the cluster is consistently lower than at its center. As a cluster passes a measurement point from head to tail, the local conductivity measured at the point exhibits an initial increase followed by a subsequent decrease. To determine the transit time difference of a cluster between two measurement points, the analysis should not focus exclusively on the transit time difference of a particular section of the cluster (such as the leading edge) between the two measurement points, but rather on the time difference for the passage of the entire cluster. Consequently, the time difference between the two signal curves (x(t) and y(t)) should be computed. This necessitates the application of a cross-correlation function to analyze the conductivity data acquired directly by this method.

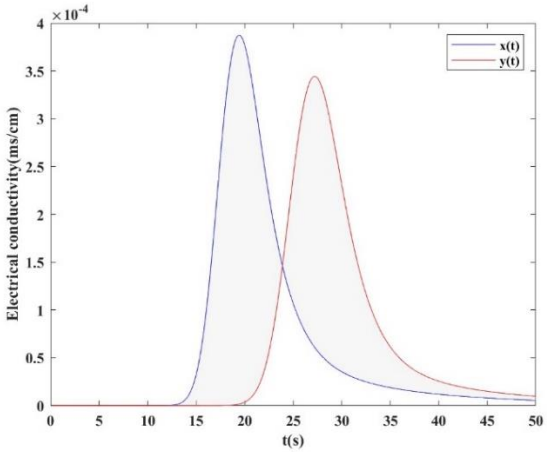

Fig. 4 Two Sets of Signal Curves

The time difference between two signal curves is calculated utilizing the principle of the cross-correlation function:

$$R_{xy}(\tau) = \int_{-\infty}^{\infty} x(t) \cdot y(t+\tau) dt \qquad (4)$$

In the equation, $x(t)$ represents the conductivity signal curve generated by the labelled fluid at the first measurement point, and $y(t)$ represents the conductivity signal curve generated by

the labelled fluid at the second measurement point. Symbol τ denotes the time shift applied to the signal $y(t)$. $R_{xy}(\tau)$ represents the sum of signal $x(t)$ and signal $y(t+\tau)$, which is delayed by τ, of all points throughout the entire time period. When $x(t)$ and $y(t)$ are very similar, and $y(t)$ is precisely the result of $x(t)$ delayed by τ_0, i.e., $y(t+\tau_0) = x(t)$, the signals $x(t)$ and $y(t+\tau_0)$ will superimpose maximally, and their product integrated over the entire time axis will achieve its maximum value (with positive signal). At this point, $R_{xy}(\tau_0)$ will correspond to the peak value, and τ_0 represents the time difference between the two signal curves.

As illustrated in Figures 5, the cross-correlation function $R_{xy}(\tau)$ reaches its peak value when the time-shifted signal y(t+τ_0) achieves maximum alignment with signal x(t). This specific time shift τ_0 corresponds to the transit time difference between the two signals.

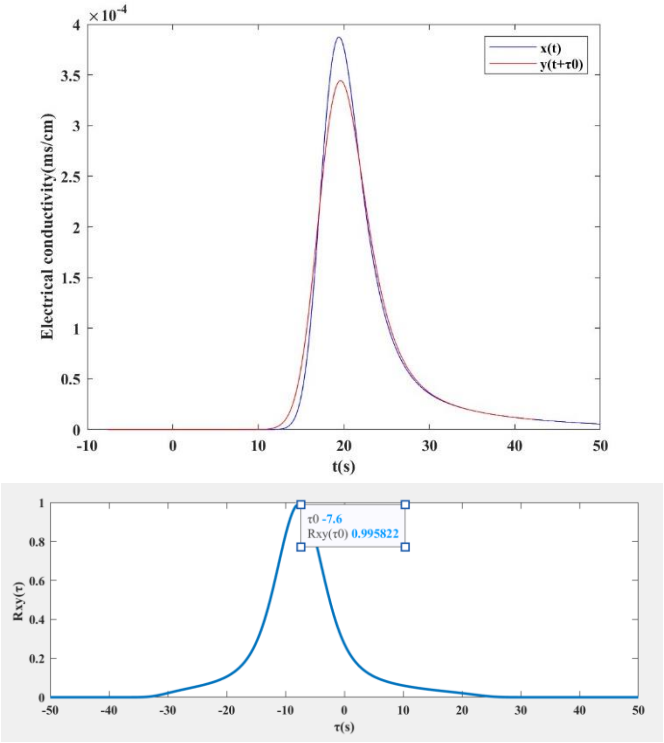

Fig. 5 $R_{xy}(\tau)$ at the Time of Maximum Overlap of the Two Sets of Signal Curves

3.3 Simulation of the measurement method

3.3.1 Overview of the simulation method: As described above, the conductivity of electrolyte solution varies linearly with concentration at certain range, meaning that the conductivity changes proportionally with the mass fraction of the conductivity liquid in water. Thus, in the numerical simulation, the curve of the mass fraction of the conductivity liquid in water as a function of time can be used to depict the migration process of electrolyte solution. The physics properties of electrolyte solution are set based on relevant literature where the viscosity of electrolytes (NaCl and KCl) and their aqueous solutions at 298.15K are listed [20, 21]. The change in conductivity between the two electrodes is simulated using the area-weighted average mass fraction of the conductivity liquid along the radial line of the measurement point cross-section. Multiple measurement points along the channel are set in the simulation, located at different distances from the channel entrance. The area-weighted average mass fraction of the conductivity liquid at each measurement point is monitored over a period of time. The time difference between two measurement points is then obtained from the mass fraction curves using the algorithm discussed above. Finally, this enables the measurement velocity of the labelled fluid cluster to be obtained.

3.3.2 Computational Fluid Dynamics (CFD) simulation: The structures of the flow channel models are based on parameters of the reactor core based on MSRE (Molten Salt Reactor Experiment) and MSBR(Molten Salt Breeder Reactor) [22, 23], with cross section including circular channel, stadium-shaped channel, and annular channel.

The fluid domains of the upper and lower plenums in the circular, racetrack, and annular flow channel models are all rectangular domains with dimensions of 8 cm × 20 cm × 5 cm. The inlet and outlet pipes used for connection of the plenums are cylindrical domains with a diameter of 4 cm, with the inlet pipes having a length of 90 cm and the outlet pipes having a length of 10 cm. The fluid domain of the flow channel is 1.5 meters long. The cross-section of the circular channel has a diameter of 2 cm, while the cross-section of the stadium-shaped channel consists of a 4 cm × 1 cm rectangle combined and two semicircles, each with a diameter of 1 cm. The cross-section of the annular channel is an annular shape with an inner diameter of 4 cm and an outer diameter of 6 cm. The main shapes are shown in Figure 6 and Figure 7. The conductivity liquid inlet is located on the pipe wall of the inlet pipe, 90 cm from the entrance of the lower plenum. The four measurement points are positioned at distances of 0.8 m, 1.0 m, 1.2 m, and 1.4 m downstream from the flow channel inlet.

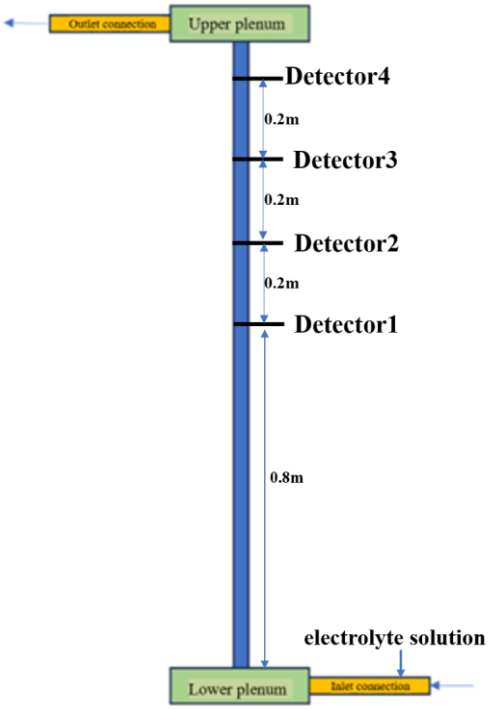

Fig. 6 Comprehensive Model of Single-Channel Test Section

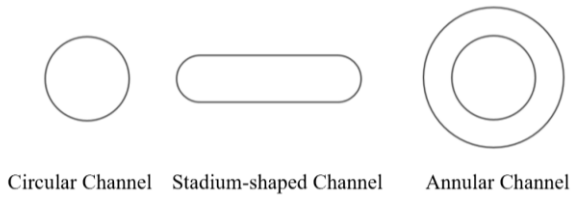

Fig. 7 Shape of the Flow Channel Cross-Section

In the practical application of this measurement method, conductivity liquid is typically injected through a small opening into the inlet pipe from the pipe wall. In the model, the conductivity liquid inlet fluid domain is a small cylindrical domain with a diameter of 2 mm, situated on the pipe wall of the inlet pipe. As a result, the size of the conductivity liquid inlet fluid domain is significantly smaller than that of other fluid domains. During the meshing process, two different grid sizes are used for the conductivity liquid inlet fluid domain and the other fluid domains. The flow channel, inlet and outlet pipes, and conductivity liquid injection domain have regular shapes and are critical computational domains. Hexahedral meshes with high accuracy and fewer elements are used for these domains. The upper and lower plenum domains serve as transitional sections between the inlet and outlet pipes and the flow channel, and are not primary computational domains. These domains primarily use tetrahedral meshes, which are well-suited for complex geometries. To ensure the accuracy of the final results in the numerical simulation, grid independence verification was conducted. Five mesh sizes, with grid counts of 5185269, 888639, 488414, 160703, and 103887, were chosen for the calculations. Computational results for five distinct mesh configurations consistently yield flow velocities on the order of 0.4 m/s at Measurement Point 2. Taking into account both computational accuracy and resource efficiency, the second mesh size was chosen for the subsequent simulation calculations.

Computational simulations were performed using ANSYS Fluent software. The shear stress transport (SST) k-ω turbulence model was selected. The species transport model was activated. The material properties for the conductive liquid corresponded to a 0.0955 mol/kg aqueous KCl solution. Its density was 1001.5 kg/m³ and its dynamic viscosity was 0.0008905 Pa·s [20]. For the boundary conditions, the inlet velocity at the inlet pipe was set to 0.1 m/s, corresponding to a mass flow rate of 0.1256 kg/s, with an initial species mass fraction of zero. The inlet velocity for the conductive liquid was specified as 0.1 m/s with duration time of 1s by setting its species mass fraction set to unity (1), otherwise zero. A pressure outlet boundary condition was applied at the outlet. The pressure-velocity coupling was resolved using the SIMPLEC (Semi-Implicit Method for Pressure-Linked Equations Consistent) algorithm. The total simulation time was 50 seconds. To investigate potential discrepancies in the inferred flow rates obtained by measuring the area-weighted average mass fraction of the conductive liquid at different radial locations, both the circular and stadium-shaped channels were instrumented with two distinct radial monitoring positions at a single measurement cross-section, while the annular channel was instrumented with four distinct radial monitoring positions at a single measurement cross-section. The distinct radial monitoring positions of the measurement cross-sections for three types of channel are illustrated in the figure 8.

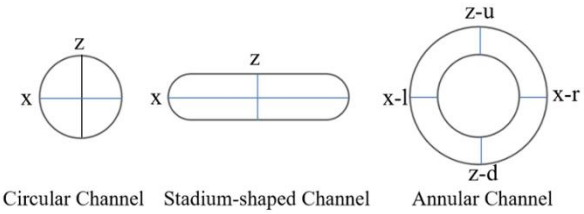

Fig. 8 Schematic Illustration of The Locations of the Measurement Points

3.3.3 Flow distribution of test channels: The axial velocity distributions along the flow direction are presented in the figure 9. Based on the simulation results, In the circular channel, the centerline velocity stabilizes and remains constant at axial positions beyond 0.7 m downstream of the inlet. For the stadium-shaped channel, centerline flow velocity achieves steady-state conditions at axial distances greater than 0.3 m from the inlet. In the annular flow channel, stable centerline velocities are maintained at all four monitored circumferential positions beyond 0.4 m downstream of the inlet. Thus this demonstrates that positioning the measurement points within these stabilized flow regions ensures stable and reliable measurement results. This establishes the fundamental basis for implementing the present cross-correlation measurement approach.

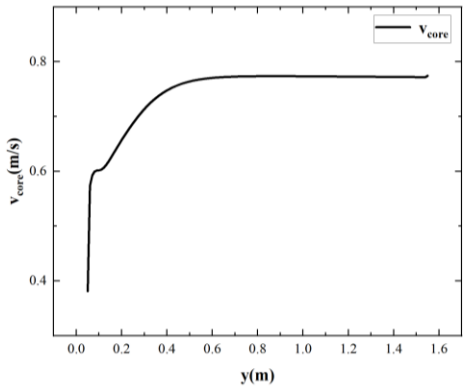

(a) Velocity Distribution Along the Flow Direction at the Center of the Circular Channel

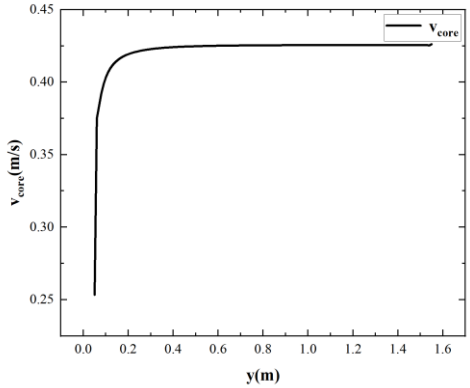

(b) Velocity Distribution Along the Flow Direction at The Center of the Stadium-Shaped Channel

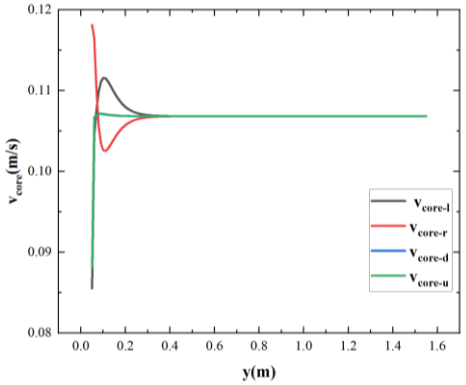

(c) Velocity Distributions of Four Radial Directions Along the Flow Direction at the Center of The Annular Channel

Fig. 9 Velocity Distribution Along the Flow Direction at the Channel Center

3.3.4 Analysis of the computational results: Figure 10 presents the variation curves of the area-weighted average mass fraction of the KCl on x radial line at four measurement points in the circular channel. Since the variation curves on both the x radial line and z radial line are almost identical at each measurement point, only one radial line is selected. The peak values of the area-weighted average mass fraction of KCl at each measurement point exhibit a gradual decrease along the flow direction, which is caused by the diffusion effect of the conductivity solution. The diffusion effect causes the signal curves produced by the electrolyte cluster at different measurement points to be not identical, which may potentially introduce a certain degree of measurement deviations. The time differences of MP1x~MP2x, MP2x~MP3x, and MP3x~MP4x are 0.496s, 0.497s and 0.497s respectively, but the difference is very small. There was no change in the relative locations where the signal peaks appeared, and the overall similarity of the curves remains almost unchanged. Therefore this does not impact the calculation of the time difference between the two signal curves using the cross-correlation function.

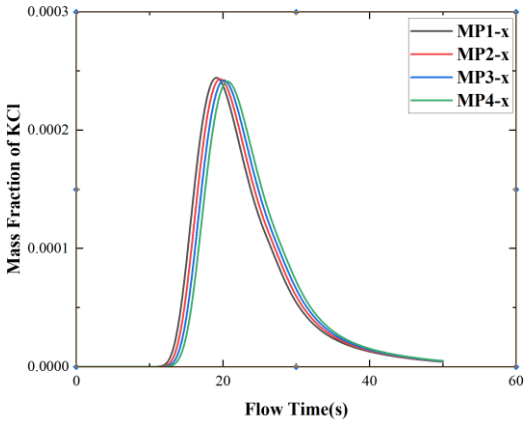

Fig. 10 The Variation of KCl Mass Fraction in the Circular Channel

Figure 11 presents the variation curves of the area-weighted average mass fraction of KCl on the x radial line at four measurement points in the stadium-shaped channel. As with the measurement results from the circular channel, the variation curves on both the x radial line and z radial line are almost identical at each measurement point, so only the variation curve on x radial line is required for calculating the time difference. The peak values of the area-weighted average mass fraction of KCl at each measurement point exhibit a gradual decrease along the flow direction due to the diffusion effect of the conductivity solution, but the differences are very small. This does not impact the calculation of the time difference between the varying waveforms using the cross-correlation function.

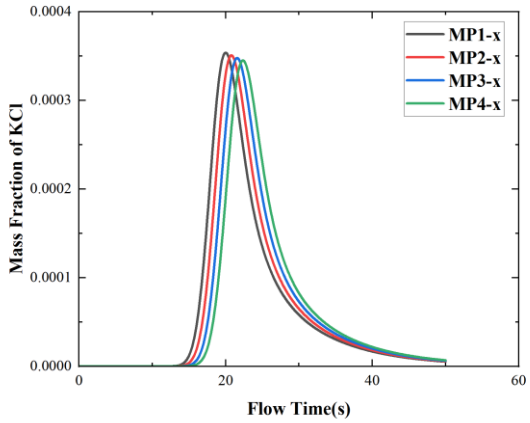

Fig. 11 The Variation of KCl Mass Fraction in the Stadium-Shaped Channel

Figure 12 presents the variation curves of the area-weighted average mass fraction of KCl on the left x radial line at four measurement points in the annular channel. On the cross-sectional plane of the same measurement points, the variation curves on radial line at the four circumferential positions of the ring are almost identical, consistent with the measurement results of the previous two types of channel. The peak value of the area-weighted average mass fraction of KCl at each measurement point shows a gradual decrease along the flow direction due to the diffusion effect of the conductivity solution, but the differences are too small to affect the calculation of the time difference between the varying waveforms using the cross-correlation function.

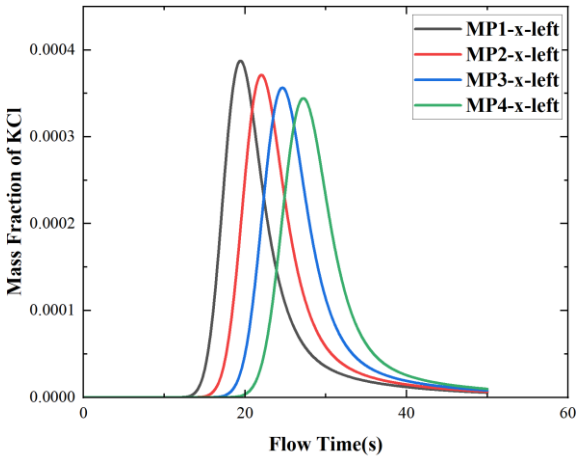

Fig. 12 The Variation of KCl Mass Fraction in the Annular Channel

The measurement time difference was calculated using the cross-correlation calculation, corresponding to the maximum similarity between the signal waveforms of the area-weighted average mass fraction of KCl at two measurement points with different spacings. The averaged time difference, calculated from the signal curves on different radial lines of the same measurement point, is shown in Figure 13. Based on the principle of mass conservation, with an inlet velocity of 0.1 m/s in the inlet pipe, the theoretical average flow velocities are 0.4 m/s for the circular channel, 0.2625 m/s for the stadium-shaped channel, and 0.08 m/s for the annular channel. Therefore, the theoretical time differences between measurement points separated by 0.2m, 0.4m, and 0.6m in the circular channel are 0.5s, 1s, and 1.5s, respectively. For the stadium-shaped channel, the theoretical time differences for the same separations are 0.762s, 1.524s, and 2.286s, respectively, and for the annular channel, they are 2.5s, 5s, and 7.5s, respectively. The measurement results at different spaced points in the three types of channel are in good agreement with the theoretical time differences. The results are converted to average flow rates and shown in Figure 14, showing only a minimal difference from the theoretical flow rates.

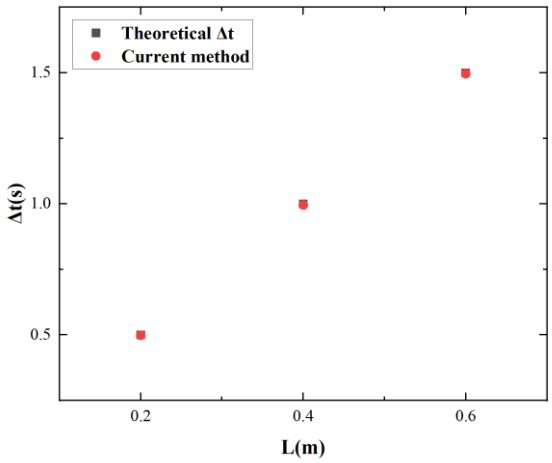

(a) Circular Channel

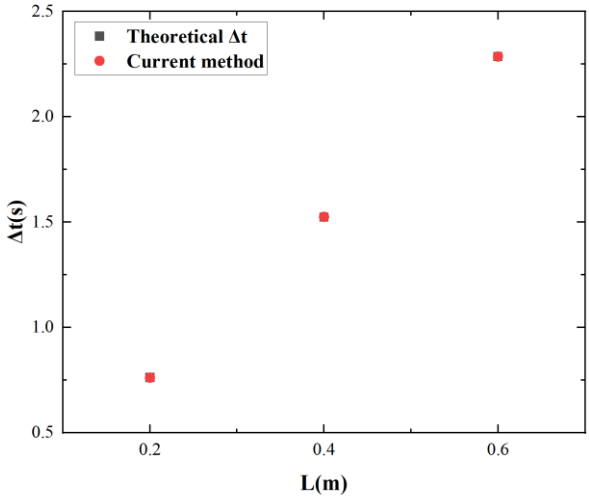

(b) Stadium-Shaped Channel

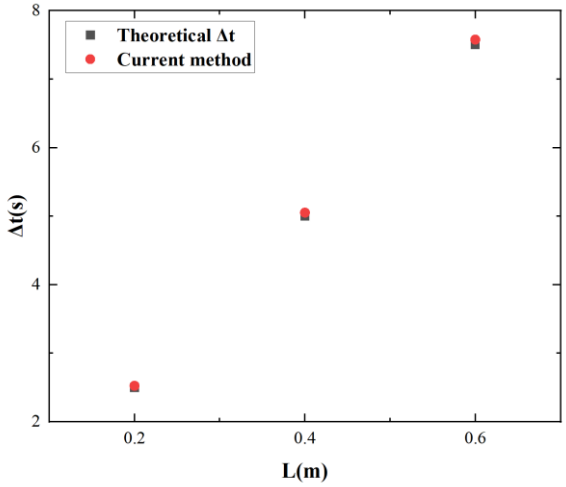

(c) Annular Channel

Fig. 13 Results of the Time Differences from Detectors at Different Locations

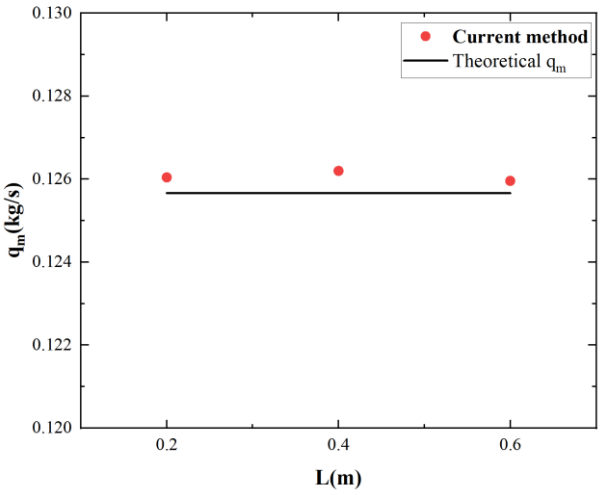

(a) Circular Channel

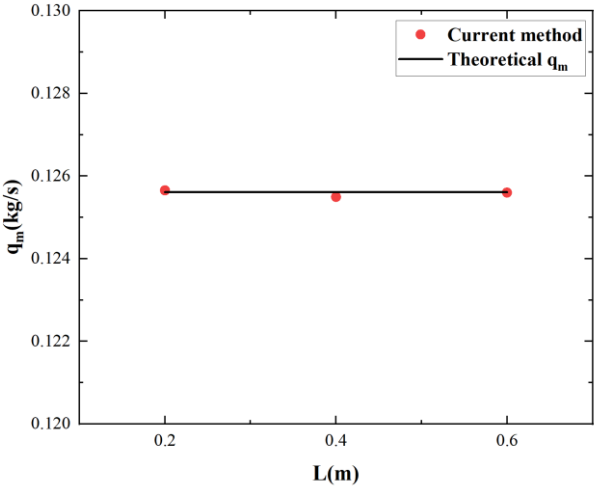

(b) Stadium-Shaped Channel

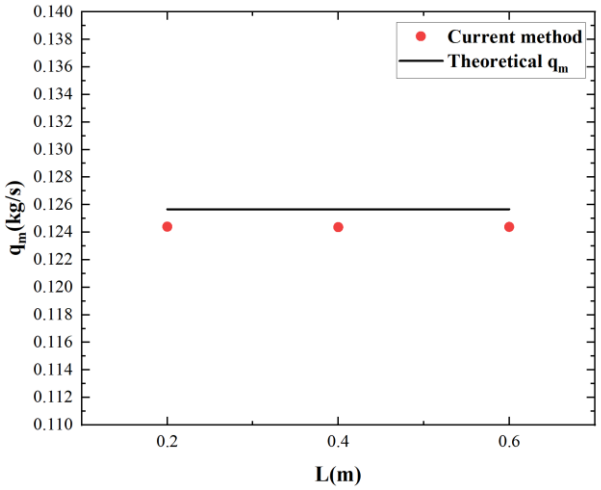

(c) Annular Channel

Fig. 14 Results of the Measured Flow Rates from Detectors at Different Locations

4. Optimization of the Measurement

The flow measurement deviations, as shown in Figure 15, indicate a maximum deviation of 0.8% for the circular channel, 0.4% for the stadium-shaped channel, and 1.26% for the annular channel, which reflects good measurement consistency and regularity. These characteristics are inclined to establish a relationship between measured results and true values, which provides the feasibility for the calibration of the measurement method.

As shown in Figure 15, the deviations between the measured results and the theoretical q_m for all radial lines of three types of channels are summarized. The scatter points form an approximately trapezoidal distribution. Measurement deviations of 0.6m ranges from -1.15% to 0.60% with both bounds being closer to zero, while measurement deviations of 0.2m ranges from -1.26% to 0.80% with both bounds being further away from zero compared to other distances. Therefore, prior to applying this method in practice, attention should be paid to optimizing the measurement point arrangement, avoiding small distances between measurement points and selecting suitable distances between measurement points for experimental validation, in order to obtain better measurement results.

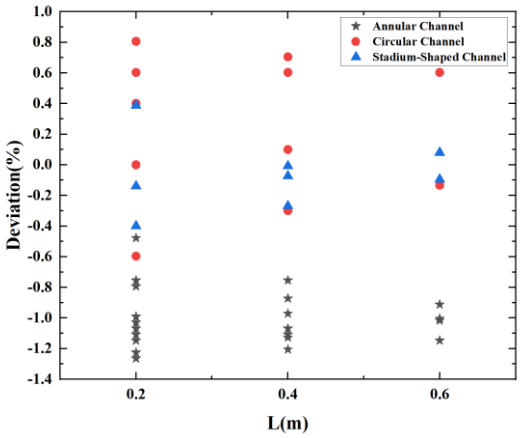

Fig. 15 Deviations in Flow Measurement across All Channels

5. Conclusion

This paper presents a flow measurement method utilizing electrolyte fluid. Additionally, it offers solutions to the critical challenges encountered throughout the measurement process in the flow distribution experiments of MSR. A computational fluid dynamics (CFD) simulation analysis is employed to analyse the application of the proposed method in different structural channels within the MSR core. The following conclusions can be drawn:

(1) An improved data analysis approach was developed for tracking the conductivity liquid, enabling precise recording the behaviour of electrolyte flow within the channel.

(2) The accuracy of the method is evaluated by means of the deviations between measured and reference values, results indicate that the current method is feasible and can be further verified.

(3) Simulation results confirm that the method has a wide range of applicability, flexible scalability, and can be applied to different structural channels.

(4) Optimization direction of layout configurations of the detector is proposed based on the results of the simulation analysis, which point out that the distance between measurement points should not be too small.

Subsequent experimental validation of the measurement method and detector design will be carried out based on the results of the current study.

6. Acknowledgements

This work is supported by the “Gansu Major Scientific and Technological Special Project under Grant (Grant No.23ZDGH001) and “Youth Innovation Promotion association. Chinese Academy of Science"(Grant No. 2020263).

7. References

[1] Dai, Z.M.:'Thorium molten salt reactor nuclear energy system (TMSR) ', Molten Salt Reactors and Thorium Energy, 2017,pp 531-540.

[2] Zhang, F., Guo, B.L.:'Molten salt reactor technology: progress, challenges, and prospect', Southern Energy Construction, 2024,pp 1-7.

[3] Sui, X., Wang, S., Yang, Z.M.:'Experimental Investigation of Flow Distribution Characteristic at Core Inlet in CENTER', Atomic Energy Science and Technology, 2020, 54,(2),pp 257-263.

[4] Peng, F., Su, Q.H., Xing, J.:' Experimental study on flow distribution and mixing at the core inlet of double-loop small module reactor', Annals of Nuclear Energy, 2020, 152,(2021),pp 1-8.

[5] Liu, B., Zhang, W., Lin, S.X.:'Scale Analysis and Model Simplification for CAP1400 R eactor

Hydraulic Simulation Test', Pressure Vessel Technology, 2017, 34,(4),pp 32-36.
[6] Ding, Z.H., LIiu, B., Lin, S.X.:'Design of hydraulic simulation test models for CAP1400 reactors', Power Equipment, 2016, 30,(3),pp 153-155.
[7] Ding, L., Chen, X., Wang, D.L.:'Experiment Research on Integral Hydraulic Simulation of ACP100 Reactor', Nuclear Power Engineering, 2023, 44,(S1),pp 29-34.
[8] Zhang, M.Q., Duan, Y.G., Yu, X.L.:'Numerical Analysis and Comparison of Overall Hydraulic Characteristics of ACPR1000+ Reactors', Nuclear Power Engineering, 2013, 34,(6),pp 52-54.
[9] Yu, D.P., Jiang, X.G., Zhang, J.W.:'Experiment Study for Flow-Induced Vibration and Flow-Distribution on Full Scale Core of China Advanced Research Reactor', Atomic Energy Science and Technology, 2008, 42,(Suppl),pp 711-714.
[10] Euh, D.J., Kim, K., Chu, I.C.:'Experimental identification for flow distribution inside APR+ reactor vessel and direction of internal structure design improvement', Journal of Nuclear Science and Technology, 2015, 53,(2),pp 1-12.
[11] Kim, K., Euh, D.J., Chu, I.C.:'Experimental study of the APR+reactor core flow and pressuredistributions under 4 — pump running conditions', Nuclear Engineering and Design, 2013, 265,pp 957-966.
[12] Wang, L.M., Zong, G.F., Yin, T.:'Experimental Investigation of Inlet Flow Distribution in the Core of a 600 MW Nuclear Reactor', Journal of Engineering Thermophysics, 1999, 20,(185-189),pp.
[13] Hong, Z.Y., Liu, S.L., Ju, S.X.:'The whole model hydraulic test of Qinshan Nuclear Power Pant reactor', Chinese Journal of Nuclear Science and Engineering, 1989, 9,(4),pp 319-327.
[14] Yang, L.S., Zong, G.F., Hu, J.:'Reactor hydraulic simulation test study of Qinshan Phase II NPP project', Nuclear Power Engineering, 2003, 24,(Suppl.),pp 208-211.
[15] Ding, Z.H., Zhang, M., Lin, S.X.:'Experiment Study on CAP1400 Core Inlet Flow Distribution', Atomic Energy Science and Technology, 2018, 52,(9),pp 1635-1640.
[16] Song, G.D., Jiang, L., Qiu, B.B.:'Study on Flow Distribution and Resistance Characteristics of Secondary Side of Intermediate Heat Exchanger', Nuclear Power Engineering, 2024, 45,(1),pp 55-59.
[17] Fu, X.C., Hou, W.H.:'The electrical conductivity of the electrolyte solution',in FU, X.C.(Ed.): 'Physical Chemistry' (Higher Education Press, 2021,6th edn.), pp. 20.
[18] Chen, L.M., Cheng, M.X., Xiao, X.F.:'Measurement of the Relationship between Conductivity of Salt Solution and Concentration and Temperature', Research And Exploration In Laboratory, 2010, 29,(5),pp 39-42.
[19] Zhao, Y.Q.:'Development and Applications of Wire Mesh Sensors'. M.S. thesis: Lanzhou University, 2018.
[20] Zhang, H.M., Zhang, S.J., Chen, G.H., et al.:'The viscosity of aqueous solutions of electrolytes (NaCl and KCl) and their mixtures at 298.15 K', Journal of Chemical Industry and Engineering(China), 1996, 47,(2),pp 211-216.
[21] Zhang, H.L., Han, S.J.:'Viscosity and Density of Water + Sodium Chloride + Potassium Chloride Solutions at 298.15 K', Journal of Chemical & Engineering Data, 1996, 41,(3),pp 516-520.
[22] Robertson, R.C.:'Reactor Primary System',in: 'conceptual design study of a single-fluid molten-salt breeder reactor', 1971edn.), pp.
[23] Robertson, R.C.:'Reactor Vessel and Core Design Data and Dimensions',in: 'MSRE design and operations report part I description of reactor design', 1965edn.), pp.